Biophysical Chemistry 189 (2014) 8–15

Contents lists available at ScienceDirect

Biophysical Chemistry

journal homepage: http://www.elsevier.com/locate/biophyschem

Mutation and low pH effect on the stability as well as unfolding kinetics of transthyretin dimer

Qiao Xue, Qing-Chuan Zheng *, Ji-Long Zhang, Ying-Lu Cui, Wen-Ting Chu, Hong-Xing Zhang *

State Key Laboratory of Theoretical and Computational Chemistry, Institute of Theoretical Chemistry, Jilin University, Changchun 130023, PR China

HIGHLIGHTS

- The acidic environment results in the loose structure of TTR dimer.
- Mutation L55P causes the disruption of strand D and makes CE-loop very flexible.
- Strand D plays an important role in protecting strand C.
- The movements of strand C is the beginning of the unfolding process.
- TTR dimer would dissociate into monomer before fibrillation.

GRAPHICAL ABSTRACT

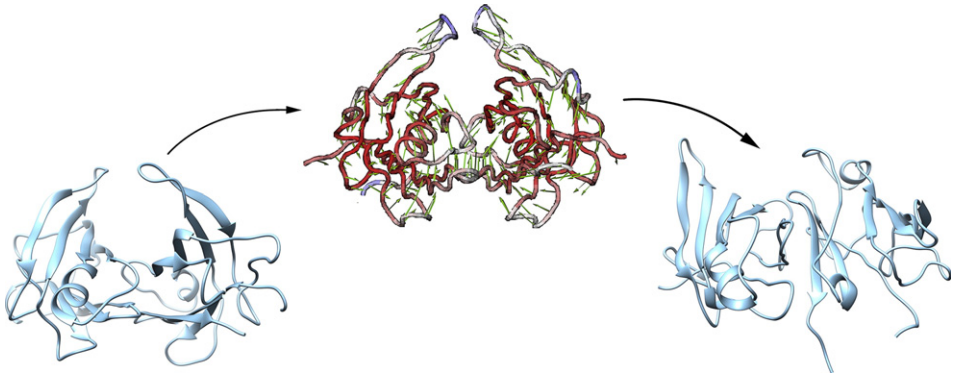

ARTICLE INFO

Article history:
Received 10 January 2014
Received in revised form 19 February 2014
Accepted 23 February 2014
Available online 3 March 2014

Keywords:
Transthyretin
Amyloid
Constant pH molecular dynamics simulations
PCA

ABSTRACT

Transthyretin (TTR) dissociation and aggregation appear to cause several amyloid diseases. TTR dimer is an important intermediate that is hard to be observed from the biological experiments. To date, the molecular origin and the structural motifs for TTR dimer dissociation, as well as the unfolding process have not been rationalized at atomic resolution. To this end, we have investigated the effect of low pH and mutation L55P on stability as well as the unfolding pathway of TTR dimer using constant pH molecular dynamics simulations. The result shows that acidic environment results in loose TTR dimer structure. Mutation L55P causes the disruption of strand D and makes the CE-loop very flexible. In acidic conditions, dimeric L55P mutant exhibits notable conformation changes and an evident trend to separate. Our work shows that the movements of strand C and the loops nearby are the beginning of the unfolding process. In addition, hydrogen bond network at the interface of the two monomers plays a part in stabilizing TTR dimer. The dynamic investigation on TTR dimer provides important insights into the structure–function relationships of TTR, and rationalizes the structural origin for the tendency of unfolding and changes of structure that occur upon introduction of mutation and pH along the TTR dimer dissociation and unfolding process.

1. Introduction

Protein misfolding and subsequent aggregation known as amyloid cause more than 20 human diseases such as Alzheimer's and Parkinson's diseases [1] Although the proteins possess different sequences and native structures, all amyloid fibrils present a similar cross-β structure [2]. In certain conditions, the structure of protein in extracellular space may

* Corresponding authors. Tel./fax: +86 431 88498962.
E-mail addresses: zhengqc@jlu.edu.cn (Q.-C. Zheng), zhanghx@mail.jlu.edu.cn (H.-X. Zhang).

http://dx.doi.org/10.1016/j.bpc.2014.02.002
0301-4622/

become unstable which can initiate amyloid fibrils step by step [3–7]. Transthyretin (TTR) is a 55 kDa tetrameric protein composed of 127-residue subunits. It is found in cerebral spinal fluid and blood plasma which plays a part in carrying the thyroid hormone thyroxine and in binding holo-retinol [8,9]. TTR amyloid diseases are triggered by the dissociation of TTR tetramer. The deposition of TTR is often associated with several diseases, including senile systemic amyloidosis (SSA), familial amyloidotic polyneuropathy (FAP), familial amyloid cardiomyopathy (FAC) and the rare central nervous system selective amyloidosis (CNSA) [9–12].

All TTR tetramers have similar overall structure. Each monomer arranges in a β-sandwich-like structure comprising β-sheets DAGH and CBEF. Based on the experimental studies, the forming pathway of TTR amyloid fibrils is conjectured like this: TTR tetramer dissociates into dimers and dimers become monomers [13]. Monomers then self-assemble to form amyloid fibrils [14].

Though many experimental studies have described the pathway of TTR dissociation [15,16], the molecular origin and the structural motifs to contribute to the unfolding and dissociation have not been rationalized at the atomic-level. Most of the previous researches focus on TTR monomer [17,18]. However, TTR dimer is an indispensable intermediate in the dissociation pathway and its information is hard to gain from experiment due to the evanescent existence [13]. To understand the mechanism of TTR dissociation comprehensively, studies on TTR dimer are necessary. To date, there has been no report to identify the atomic-level mutant conformations of TTR dimer, as well as the structural characteristics at low pH environment. To this end, molecular dynamics (MD) simulations may be used to investigate the processes of unfolding and aggregation to gain the atomic level information [19–22]. The dynamic investigation on TTR can provide important insights into the structure–function relationships of TTR as well as the tendency of unfolding and change of structure.

In general, human TTR is stable under physiological conditions. Nonetheless, it is easy to dissociate at low pH and reaches the fastest speed of dissociation at pH 4.4 [23]. To accelerate the unfolding process and investigate the effect of acidic conditions on TTR stability, constant pH molecular dynamics (CpHMD) simulations are used to survey the dissociation of TTR at neutral and acidic pH, respectively. In addition, human TTR mutant L55P is the most amyloidogenic mutant among numerous mutations which would form amyloid fibrils under physiological conditions [24]. At pH 4.4, L55P dissociates and forms amyloid fibrils rapidly, which is suitable to observe the unfolding pathway using CpHMD simulations for a limited time. In this article, 20 ns CpHMD simulations were performed to investigate the unfolding processes of human TTR dimer affected by mutation and acidic environment. These researches would shed new light on the mechanism of TTR amyloidogenesis. In addition, our investigation would contribute to the understanding of how protein folding and misfolding are determined by certain conditions, which has always been a main problem in structural biology.

2. Method

The structures of human wild-type TTR (wtTTR) and mutant L55P (L55P) were obtained from the Protein Data Bank (PDB ID: 3W3B, 3DJZ). The crystal structure misses 7 residues at N-terminal and 2 residues at C-terminal. Thus each monomer has 118 residues. Because the missed residues have no structural information and fail to have any function, we do not add these residues to keep the accuracy of MD simulation. Discovery Studio (DS) software package was used to refine and repair the structure [25].

2.1. Constant pH molecular dynamics simulations method

CpHMD is a useful method to describe the protonation state correctly at a given pH [26]. Combining MD and Monte Carlo (MC) sampling [27,28], CpHMD can handle the problem that the protonation states of titratable residues would not change during the traditional MD simulations. CpHMD was performed using the SANDER module of the AMBER 11 with force field ff03 [29,30]. Generalized Born (GB) solvation model (igb = 2) was used to describe the aqueous environment [31–33]. The GB model has been proved to be good for various biomolecular systems and it is appropriate for the CpHMD simulations [28]. All ASP, GLU and HIS residues names were changed to AS4, GL4 and HIP, respectively. This ensured that the prmtop file would have a hydrogen atom defined at every possible point of protonation. All CpHMD simulations were carried out at pH 7.0 and pH 4.4, using a 30 Å cutoff value for non-bonded interactions [28]. Salt concentration (Debye–Hückel based) was set at 0.1 M. The SHAKE algorithm was used to constrain all bonds involving hydrogen, allowing a time step of 2 fs. The entire system was submitted to 2000 steps of steepest decent minimization followed by 3000 steps of conjugate gradient minimization. Then, the entire system was submitted to heat from 0 K to 310 K in 300 ps. After the heat process, the system went through a 500 ps equilibrium MD simulations process. Finally, the production runs were carried out for 20 ns with 2 fs time step. All trajectories were recorded every 2 ps.

2.2. MD trajectory analysis

We analyzed the trajectories using several orders of AMBERTOOLS. The root-mean-square deviation (RMSD) value is a useful estimation for quantifying the conformational changes of the same proteins. In this study, Cα-RMSD was calculated for all the systems. To evaluate the local structure fluctuation of helixes and β-sheets, the hydrogen bond populations were calculated. The hydrogen bond is defined if the distance between donor and accepter is shorter than 3.5 Å and the angle is larger than 120°. In the present study, 20 ns MD simulations are performed for the four systems, which can generate 10,000 snapshots. Cluster analysis is the task of grouping a set of snapshots in such a way that snapshots in the same group (called a cluster) are more similar to each other than to those in other groups (clusters). The cluster analysis of the protein conformations is performed using the averagelinkage as the clustering algorithm, and backbone atom RMSD as the distance metric. The averagelinkage algorithm is recommended in all cluster algorithms [34]. It can be summarized as follows: under the averagelinkage algorithm, the distance from one cluster to another is defined as the average of all distances between individual points of the two clusters. At each iteration step, the two closest clusters are merged. This merging continues until the desired number of clusters is obtained (here is 5). The Pymol and Chimera software were used for the visualization of many files in this study [35,36].

2.3. Cross-correlation analysis

The cross-correlation can be used to probe the inter-domain coupling of proteins during the MD simulations. In general, C_{ij}, cross-correlation coefficient, was calculated to reveal the correlated motion between pairs of residues. All the 20 ns simulations of the dimers were selected to be calculated by the following equation:

$$C(i,j) = \frac{\Delta r_i \times \Delta r_j}{\left(\left\langle \Delta r_i^2 \right\rangle \left\langle \Delta r_j^2 \right\rangle\right)^{1/2}} \quad (1)$$

In Eq. (1), Δr_i and Δr_j are the displacement vectors for atom i and atom j, respectively. The angle bracket represents an average over the sampled period. In our calculations, $C\alpha$ of the residues was chosen to represent the correlated motion of a residue pair [37]. The value of C_{ij} fluctuates from −1 to 1. Positive C_{ij} values represent a correlated motion of a residue pair, while the negative values describe an anticorrelated motion.

2.4. Principal component analysis

Principal component analysis (PCA) is used to separate a protein's conformational space into the essential subspace containing several degrees of freedom that describe the motions of the proteins [38]. PCA uses a covariance matrix constructed with structures sampled from the molecular dynamics simulations. By diagonalization of a covariance matrix of the coordinates of the systems, the motions of a structure along the trajectory are determinate. To obtain the dominant motion over a MD simulation, trajectory would be projected along the direction described by a selected eigenvector. Through calculating the two largest projections on the average structure, the primary moving direction of the protein can be obtained. PCA was performed using ProDy software [39]. Three-dimensional structural snapshots were visualized using VMD and its plugin NMWiz [39,40].

3. Results and discussion

3.1. Different stability under neutral and acidic conditions

The TTR dimer in this study contains two monomers, named A and B. Each monomer consists of one α-helix (residues 75–82) and eight β-strands (residues 12–18, 28–35, 41–49, 54–55, 67–73, 91–97, 104–112, and 115–123, denoted as A, B, C, D, E, F, G, and H, respectively), as shown in Fig. 1. For clarity, wild-type TTR dimer at pH 7.0, wild-type TTR dimer at pH 4.4, mutant TTR L55P at pH 7.0 and mutant TTR dimer at pH 4.4 are referred to as WT7.0, WT4.4, L55P7.0, and L55P4.4, respectively.

Fig. 2a shows the variation of the Cα-RMSD curve of each dimer from the initial structure. During the 20 ns MD simulations, the RMSD value of each dimer reached equilibrium with an average value of 2.64 (standard deviation 0.27), 2.94 (0.36), 2.62 (0.38) and 8.28 (2.86) for WT7.0, WT4.4, L55P7.0 and L55P4.4, respectively. In general, compared to the TTR dimers at neutral pH, the RMSD values of the TTR dimers in the acidic environment are larger. Moreover, WT7.0, WT4.4, and L55P7.0 have reached the equilibrium quickly. However, the RMSD of the trajectory of L55P4.4 rapidly increased and fluctuated after 3.3 ns. After 4.5 ns, the RMSD value of L55P4.4 increased further and showed a larger departure from the initial structure. Fig. 2b shows the distributions of the radius of gyration (*Rg*) as a function of time. Both wild-type TTR and mutant at pH 4.4 showed larger *Rg* values than those at neutral pH. In particular, the *Rg* of WT4.4 was slightly larger than WT7.0, and *Rg* of L55P4.4 was quite different from L55P 7.0. This result indicates that the global structures of the TTR dimers were not conserved under acidic conditions, particularly for L55P. To further compare the structural differences, we analyzed the RMSF of backbone atoms averaged for each residue, as shown in Figure S1. It clearly shows that the fluctuations of the residues, particularly for those in strands A–D, are larger at pH 4.4. The mutant also has larger RMSF values compared to wtTTR.

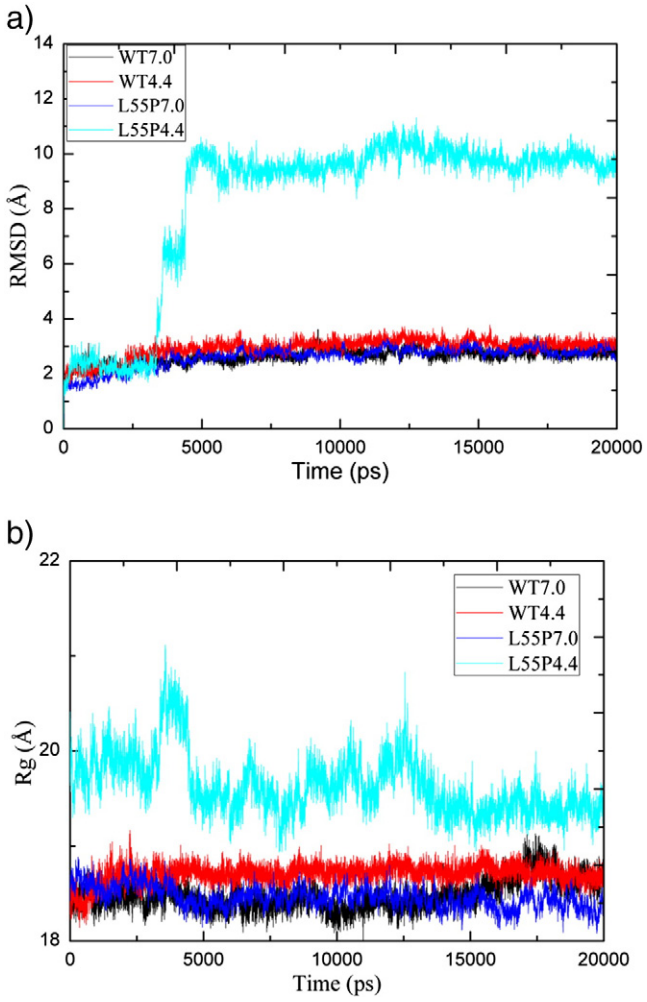

Fig. 2. Structural characteristics of WT7.0 (black), WT4.4 (red), L55P7.0 (blue) and L55P4.4 (cyan). (a) Cα-RMSDs from the initial structure as a function of simulation time. (b) Radius of gyration as a function of simulation time.

Figure S2 shows the analysis of secondary structure. In the wtTTR at different pH values, the secondary structures clearly remain unchanged under the acidic conditions. This significantly changed the secondary structures. At pH 7.0, strands C and H of L55P were unstable during the simulations. At pH 4.4, the secondary structures of L55P were destroyed further. In particular, the DAGH β-sheets of monomer A were not stable, and strand H almost disappeared after 4 ns. For monomer B, strands A and D are unstable. This result indicates that the mutation clearly affected the secondary structure, and the acidic conditions enhanced this effect.

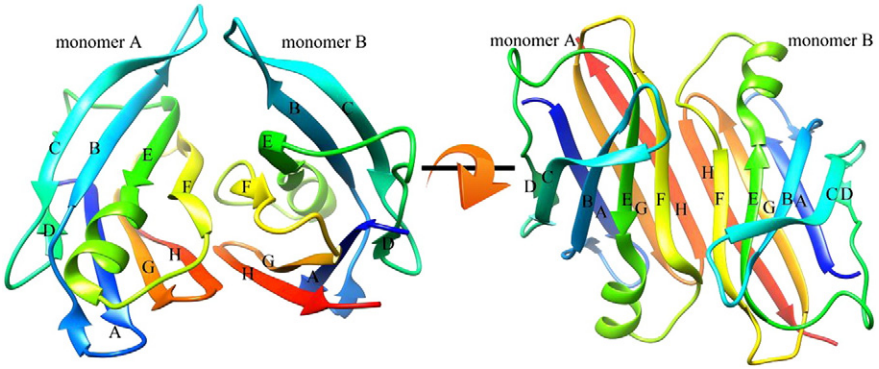

Fig. 1. Schematic representation of transthyretin dimer composed of monomer A and B. Each monomer has two sets of β-sheets (DAGH and CBEF).

Table 1
Hydrogen bonds between monomer A and monomer B of WT7.0 and WT4.4.

WT7.0	Donor	Acceptor	%Occupancy	WT4.4	Donor	Acceptor	%Occupancy
AEFloop-BF	F87	T223	37.94	AF-BH	E92	Y243	7.99
AEFloop-BF	E89	T223	6.91	AF-BE	E92	K197	5.2
AF-BH	E92	Y243	87.01	AF-BEF	V94	H215	10.13
AF-BE	E92	K197	33.2	AGHloop-BH	Y114	T246	7.57
AH-BH	S115	T246	8.59	AH-BH	S115	T246	14.47
AH-BH	Y116	T245	27.77	AH-BH	Y116	T245	6.7
AH-BH	S117	S244	35.39	AH-BH	S117	S244	34.65
AH-BH	T119	S242	12.19	AH-BH	T118	S242	6.22
BEFloop-AG	F214	Y105	23.42	AH-BH	T119	S242	10.49
BEFloop-AF	E216	T96	27.28	BEFloop-AF	F214	T96	9.47
BF-AH	E219	Y116	57.13	BEFloop-AF	E216	T96	17.61
BF-AEFloop	V221	H88	64.48	BGHloop-AH	Y241	T119	8.07
BH-AH	S242	T119	6.85	BH-AH	S242	T119	9.46
BH-AH	Y243	T118	19.03	BH-AH	Y243	S117	7.44
BH-AH	S244	S117	27.2	BH-AH	S244	S117	33.24
BH-AH	T245	S115	9.54	BH-AH	T245	S115	5.42
BH-AH	T246	S115	6.42	BH-AH	T246	S115	14.89

3.2. pKa measurement of the titratable residues and the corresponding changes in the structure

It is well known that a change in the protonation state of a titratable residue can dramatically change the protein conformation. Acidic environment changes the pKa of the residues of TTR. The computed pKa of each titrable residue is listed in Table S1. The calculations of pKa using AMBER11 are accurate when the absolute value of the offset is less than 2.0. Therefore, we choose the residues located in this range for the analysis. Hydrogen bonds prevent titratable residues from protonating, thus leading to low predicted pKa values. The hydrogen bond donor (offer oxygen atom) has a low pKa value and the hydrogen bond acceptor (offer hydrogen atom) has a high pKa value. Table S2 shows that for WT7.0 and WT4.4, residues Glu42, Glu61, Glu62, Glu63, Glu188, and Glu193 show a notable change in pKa value. The reduced/raised pKa values are consistent with the changes in their hydrogen bonds. For instance, Glu42 has a higher pKa value in WT7.0 than WT4.4. Therefore, the hydrogen bond formed by Glu42 has less occupancy along the trajectory in WT7.0. Such a situation was also observed in L55P. In addition, all the residues with significantly changed pKa values were located at strands C and D and nearby loops. These residues affect the local structure as discussed below.

3.3. Intermonomer hydrogen bond deficiency due to the mutation and acidic conditions

The hydrogen bonds between strands F and H in monomer A and B mainly stabilize the TTR dimer. Thus, the stability of the intermonomer hydrogen bonds is an important criterion role to evaluate the stability of the TTR dimer. The intermonomer hydrogen bonds of the four systems are listed in Tables 1 and 2. The inter-monomer hydrogen bonds are different in the four systems. For WT7.0, a total of 17 hydrogen bonds are present between monomers A and B. All these hydrogen bonds are formed at strands F and H and EF-loop. All these regions are located at the interface of the two monomers. Only one hydrogen bond is formed at strand G (Tyr214–Tyr105); however, the residue Tyr 105 is the last residue of strand G and is located close to strand H. Thus, these hydrogen bonds fix the positions of the two monomers and stabilize the structure of the TTR dimer, which is consistent with the previous research [41]. Compared to WT7.0, L55P7.0 has fewer hydrogen bonds between monomers A and B. Tables 1 and 2 show nine hydrogen bonds between the two strands H in WT7.0, while only seven hydrogen bonds are present in the same place of L55P7.0. In addition, the occupation of the intermonomer hydrogen bonds of L55P7.0 is smaller than that of WT7.0. These results indicate that the contacts of monomers A and B in WT7.0 are closer than L55P7.0.

Table 2
Hydrogen bonds between monomer A and monomer B of L55P7.0 and L55P4.4.

L55P7.0	Donor	Acceptor	%Occupancy	L55P4.4	Donor	Acceptor	%Occupancy
AEF-BG	F87	Y232	16.44	AEF-BF	E89	T223	7.11
AEF-BF	E89	T223	40.44	AG-BH	A108	T246	54.82
AF-BH	E92	Y243	35.2	AH-BH	T118	S242	17.19
AF-BEF	V94	H215	8.28	AH-BH	T119	S244	61.36
AH-BH	S117	S244	30.54	AH-BGH	A120	Y241	68.64
AH-BH	T118	S242	5.01	BH-AH	S242	T119	56.1
AH-BH	T119	S242	6.51	BH-AH	S242	T118	7.5
BEF-AF	F214	T96	20.07	BH-AH	T245	S117	69.1
BF-AH	E219	Y116	85.28	BH-AH	T245	S115	8.77
BH-AH	S242	T119	6.53	non-native			
BH-AH	S244	S117	28.48	AAB-BFG	A19	N225	9.05
BH-AH	T245	S115	11.47	AAB-BG	A19	Y232	5.52
BH-AH	T246	S115	12.89	AAB-BFG	A19	S227	5.5
non-native				AFG-BAB	D99	R148	24.21
BEF-AB	E216	K35	15.23	AG-BH	A108	T246	54.82
BEF-AC	E216	W41	5.94	BBC-AH	N124	R148	6.37
BEF-AC	H217	W41	13.05	BF-AG	T223	S112	18.94
BF-AE	E219	K70	31.96				
BGH-AFG	P240	R103	10.33				

At pH 4.4, the intermonomer hydrogen bonds become unstable for wtTTR. Compared to WT7.0, although the number of hydrogen bonds is similar at different pH values, the occupations of all the hydrogen bonds in WT4.4 decreased dramatically. Table 1 shows that only two hydrogen bonds of WT4.4 occupied more than 20% of the trajectory. However, 10 hydrogen bonds in WT7.0 occupied more than 20% of the trajectory. Compared to wtTTR, most of the intermonomer hydrogen bonds of L55P4.4 disappeared. Only 8 hydrogen bonds are present between the strands F/H of the two monomers. This result indicates that under acidic conditions, the two monomers of the TTR dimer are not as close as those under neutral conditions. The acidic condition has a significant effect on mutant L55P.

3.4. Non-native intermonomer hydrogen bonds brought by mutation

The structure of TTR clearly shows that strands C, D, F, and H are located outside, while strands A, B, E, and G are located inside. Strands F and H and the nearby loops compose the interface of monomers A and B. The hydrogen bonds in the interface can reinforce the contacts of the two monomers. However, some non-native hydrogen bonds are present which are not observed in wtTTR, as shown in Fig. 3 and Table 2. For wtTTR, all the intermonomer hydrogen bonds are located at the interface under neutral or acidic conditions. For L55P7.0, five non-native hydrogen bonds are formed in the EF-loop (monomer B) – strand B (monomer A), EF-loop (B) – strand C (A), strand F (B) – strand E (A), and GH-loop (B) – FG-loop (A). The formation of these hydrogen bonds indicates that the structures of L55P monomers are different with the initial structure. This also indicates that the positions of the two monomers have changed. Clearly, the mutation significantly affected the structure of the TTR dimer. For L55P4.4, seven non-native hydrogen bonds are present. Obviously, the acidic conditions strengthen the mutation effect on the structure. Under acidic conditions, monomers A and B fail to remain intact and the positions of some residues changed significantly in L55P. These non-native hydrogen bonds induce the instability of L55P.

3.5. Structural origin for conformational changes under acidic conditions and mutation

To further characterize the structural details of the unfolding process, clustering analysis of the structures was carried out. Each trajectory was divided into five clusters using the averagelinkage algorithm. In these 5 clusters, 5 snapshots were chosen to be the representative structures of clusters and named them as follows, C0, C1, C2, C3 and C4. C0 represents the initial structure. The RMSD values of C1, C2, C3 and C4 to C0 increase in sequence. Fig. 4 shows the representative structure of the most populated cluster and its comparisons to the first representative structure, C0.

At pH 7.0, the most popular cluster of WT7.0 is C2 containing 43.4% of the total population. The RMSD value of C2 to the first structure C1 is 1.60 Å. In general, the structural differences among the clusters are not clear. The situation in L55P7.0 is different than WT7.0. The populations of C2 and C4 are similar containing 36.0% and 39.8%, respectively. In addition, the RMSD values of C2 and C4 to the initial structure are 2.69 Å and 3.08 Å, respectively. These results show that the conformation of L55P7.0 has relatively clear changes. From the comparison of the representative structures of C4 and C0, the detailed structural information that induces the changes can be identified. The disruption of strand D significantly affected the entire structure even at neutral pH. This makes the CE-loop very long and flexible, thus locating it outside the dimer. Thus, the inner residues are easily exposed to water. The CBEF β-sheets of L55P are not as close as wtTTR to AGH β-sheets.

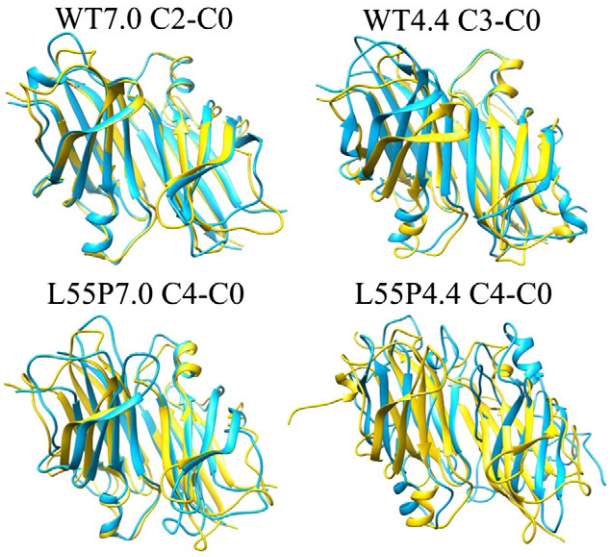

Fig. 4. Comparisons of the most populated cluster structure (cyan) and the first cluster structure C0 (yellow) for WT7.0, WT4.4, L55P7.0 and L55P4.4. The most populated cluster structures refer to the representative structures during the MD simulations, and the first cluster structures refer to the initial structures for each system.

At pH 4.4, the structural changes in the protein are more evident than those under neutral conditions. C3 is the most popular cluster containing 84.0% of the total population in WT4.4. The RMSD value of C3 to the initial structure, C1, is 2.77 Å, which is larger than that at neutral pH. Fig. 6 shows that the flexibility of strands C and D is the main reason to relax the entire structure. For L55P4.4, the most popular cluster C4 contains 58.0% of the total population. The RMSD value of C4 to C0 is 9.81 Å. The cluster analysis shows that the structure of L55P4.4 undergoes an enormous change. Because of the disruption of strand D in L55P4.4, the CE-loop is labile. Acidic conditions would also loosen the structure. Strands C in the two monomers are partially disrupted. The CBEF β-sheets fail to maintain their initial form. Fig. 4 shows a trend of retroflexion in both the monomers.

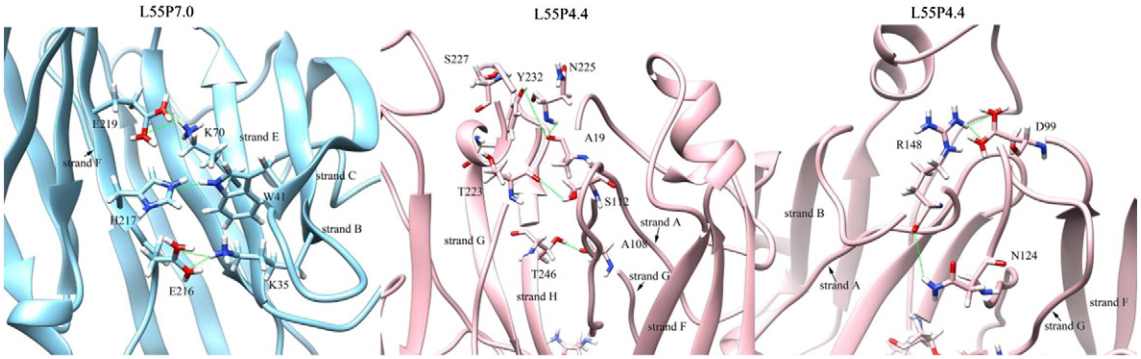

Fig. 3. Non-native intermonomer hydrogen bonds in L55P7.0 and L55P4.4.

3.6. Correlated motions of the residues in the four systems

The above analysis indicates the entire change in the conformation. To better understand the internal motions of the proteins and residues, the correlated motions of the residues in the dimers were investigated. Clearly, the interactions among the four dimers are different, see Fig. 5. Within each monomer, the residues only show positive correlation movements with the adjacent residues in WT7.0. The situation in L55P7.0 is rather different. Strand C and CE-loop show positive correlation with all the other nearby strands. The disruption of strand D makes the CE-loop very flexible and affects the stability of strand C. The fluctuation in these two regions can induce the motions of the entire monomer. Thus, the mutation of L55P clearly affected the stability of the monomer. At pH 4.4, the positive correlation movements of the adjacent residues in wtTTR are smaller than those at neutral pH. This result shows that the structure at pH 4.4 is not as close as that at pH 7.0. The correlation analysis of L55P4.4 also indicates that the acidic conditions would decrease the correlation movements within each monomer.

The mutation and acidic environment not only affect the correlation movement within the monomer, but also affect the relative correlation movement between the two monomers. For WT7.0, the only correlation movements concentrate on strands F and H between the two monomers. L55P7.0 has other correlation movements. Fig. 5 shows that the EF-loop of monomer B has positive correlation with strand C and F, and CE-loop and FG-loop of monomer A. Strand C in one of the monomer has a negative correlation with the CE-loop in the other monomer. At pH 4.4, the correlation movements of strands F and H in wtTTR are smaller than those at pH 7.0. The correlation movements of L55P at pH 4.4 are disordered. Many positive correlation movements were observed in strands B, C, F, H and the loops near them. This indicates that these domains are flexible. The cross-correlation results indicate that the correlation motion between monomers A and B would be influenced by both mutation and acidic environment. The acidic conditions can relax the structure of TTR, resulting in the loss of correlation motion between strands F and H in monomers A and B. The new correlation motion in L55P shows that the mutation causes the structural changes in the protein.

3.7. Relative motion of dimers and the unfolding process

To quantitatively identify the relative motion of the dimers, PCA was carried out for each system. In general, the two most principal components (named PC1 and PC2) represent more than 50% of the overall fluctuations for WT7.0, WT4.4, L55P7.0 and L55P4.4. To clearly show the motion of TTR, the structural variation along the first principal component is shown in Fig. 6. It is easy to find the notable motions in the four system points on the different parts of the structures. For WT7.0, the most distinctive feature is the movement of the CD-loop, strand D and DE-loop. The fluctuations in the other structures are small.

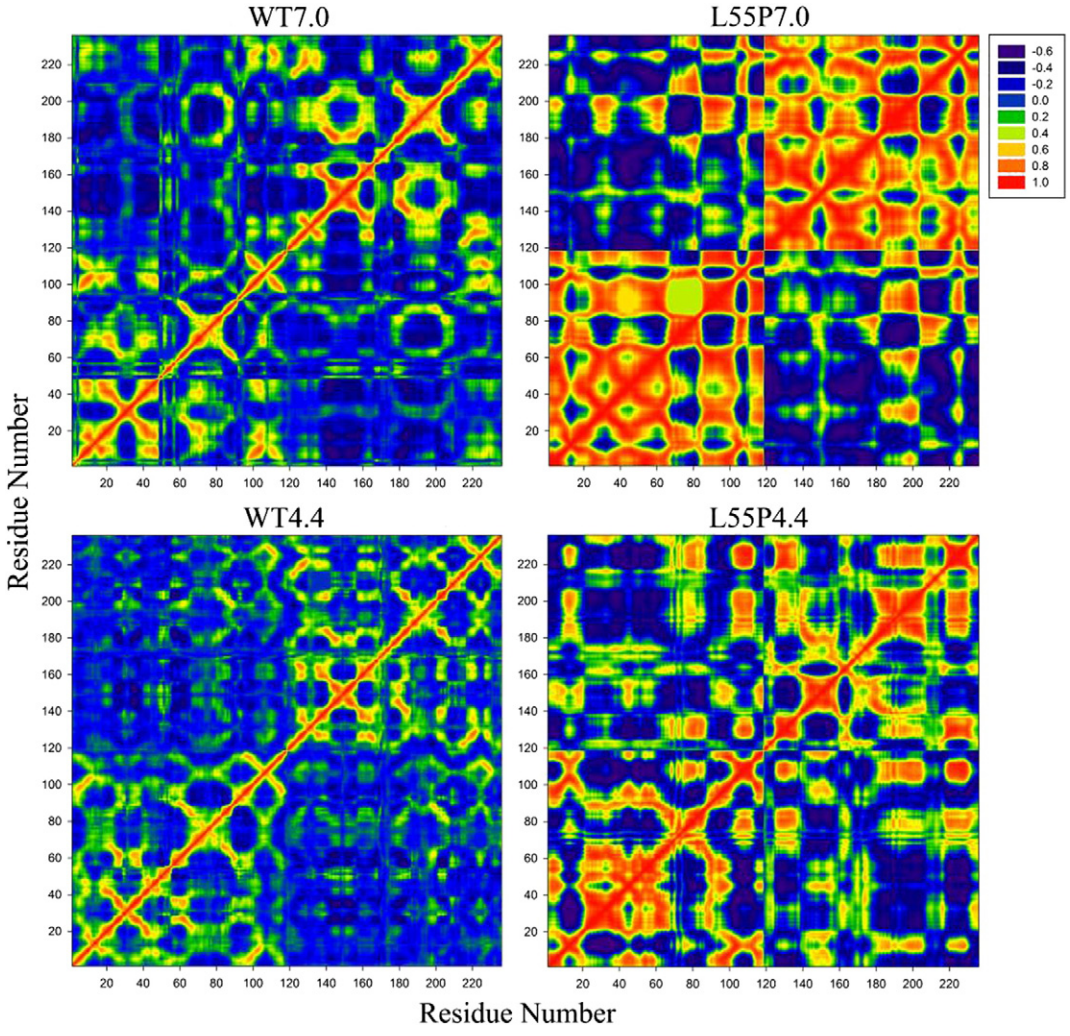

Fig. 5. Cross-correlation matrices of the coordinate fluctuations for Cα atoms of WT7.0, WT4.4, L55P7.0 and L55P4.4 around their mean positions during the 20 ns simulations. Residues 1–118 refer to monomer A and residues 119–236 refer to monomer B. Each image can be divided into 4 parts: correlation of monomer A interior (lower left), correlation of monomer B interior (upper right) and correlation between monomers A and B (upper left and lower right). Positive correlations in descending order are shown in red, orange, and yellow. Anti-correlated motions are shown in blue.

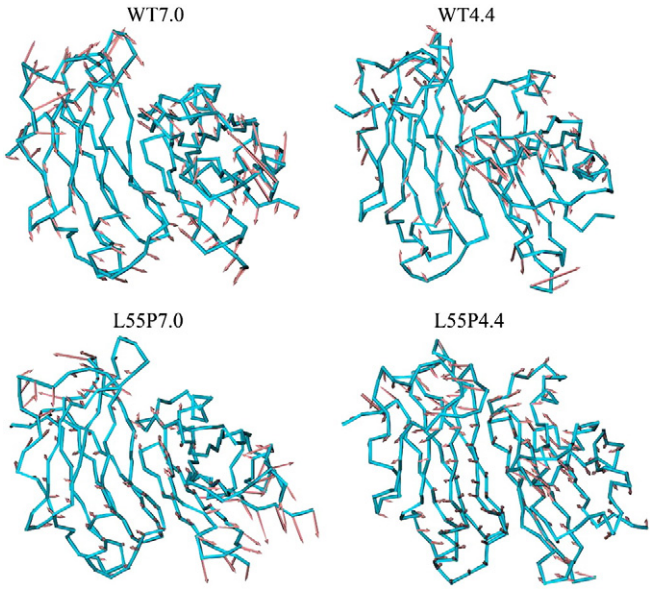

Fig. 6. A porcupine plot in stereo showing the TTR dimers with cones signifying the first eigenvectors movements.

Compared to WT7.0, L55P7.0 has more obvious movement at strands C–E and A. The above analysis shows that the mutation disrupts strand D and makes strands C–E very flexible. The PCA analysis indicates that strand C and CE-loop move down towards the β-sheet double layer. At pH 4.4, strands B and C of WT4.4 move down towards the β-sheet double layer. Simultaneously, strands E and F slightly move upwards. This conformational change results in the flat CBEF β-sheets. The motion of L55P4.4 with a large movement of the overall protein combines the effect of mutation and acidic environment and magnifies these effects. Fig. 6 shows that strands B and C and CE-loop move down towards the β-sheet double layer. Strand C was found to move down towards the β-sheet in all the four systems except WT7.0. This movement is consistent with that required for the "edge exposure" model proposed by Yeates et al. [42]. All the other strands in L55P4.4 move upwards. In addition, strands E and F are pushed outwards. The overall motion of L55P4.4 shows an obvious reverse trend for monomers A and B, thus separating each other. This motion proves the conjecture of the experimental result that the dimer would dissociate into the monomer before the fibrillation.

We also projected the trajectories onto the PC space, which describe the motions of the proteins along the trajectories. Fig. 7 shows the projections of the TTR dynamics of all the four systems, along with the projection of the initial structural conformation for reference. WT7.0, WT4.4 and L55P7.0 are more restrained than L55P4.4. The distributions of the four systems in the PC space are different from each other. We obtained the snapshot from the ensemble region for all the systems and combined the cluster analysis to represent the motion of the conformation. The results also show that the fluctuation of strands C and D and the loops nearby induce the structural changes, which is consistent with the above analysis and the cluster analysis.

4. Conclusion

By performing all-atom MD simulations with GB solvation model at constant pH, we have investigated the atomic-level structural variations for human TTR dimer and mutant to understand the effect of the mutation and low pH value on the unfolding process. Compared with wtTTR dimer at neutral pH (WT7.0), other systems (WT4.4, L55P7.0 and L55P4.4) have fewer hydrogen bonds between the interface of two monomers and more non-native hydrogen bonds. These non-native hydrogen bonds induce the instability of dimers. The acidic environment would result in the loose structure of TTR dimer. The mutation Leu55 to Pro55 causes the disruption of strand D. The labile CD-loop

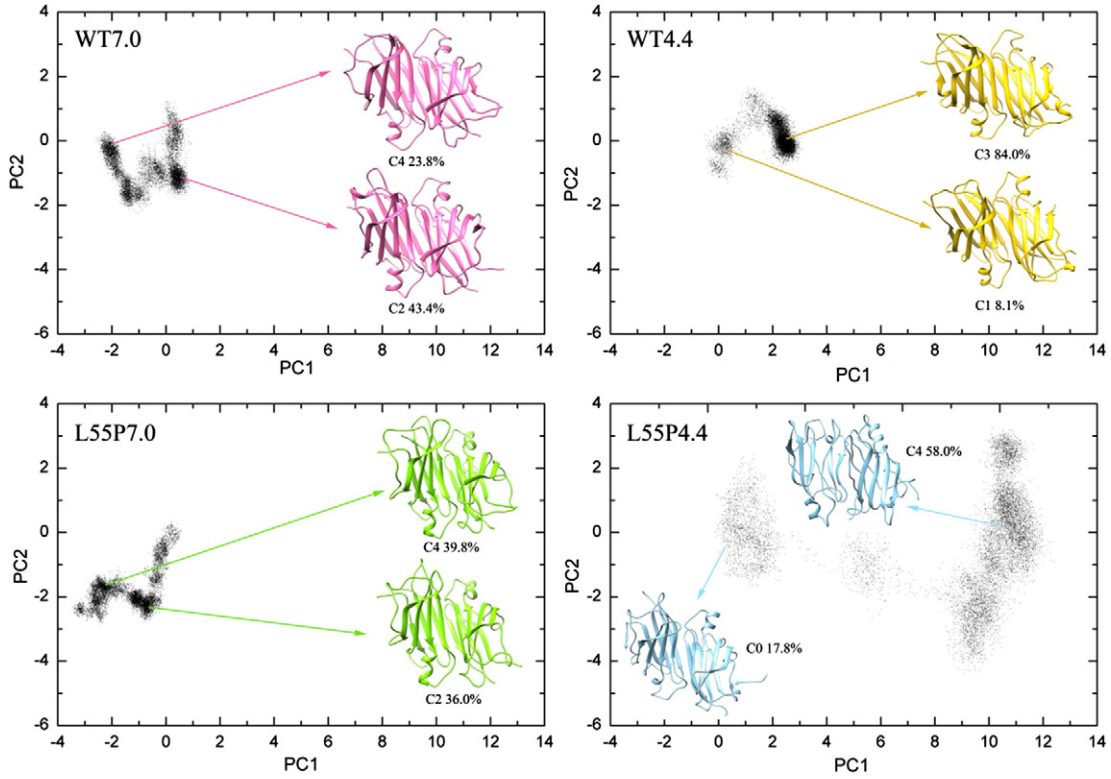

Fig. 7. Projection of the structures onto the subspace spanned by principal modes PC1 and PC2 extracted from PCA. The structures correspond to the most two populated clusters are also labelled.

and DE-loop make the edge region unstable in human TTR dimer then cause the disruption of strand C. It is inferred that the starting point of dissociation from dimer to monomer is the disruption of strands C and D. Strand D plays an important role in protecting strand C. When strand D is broken, the labile strand C causes the motion of β-sheet double layer and subsequently the separation of the two monomers. Overall, the results provide the tendency of unfolding pathway and render the structural motif and molecular origin to rationalize the experimentally conjectural dissociation process by single point mutation and acidic environment. Furthermore, the conclusion would also contribute to further understanding the mechanism of TTR amyloidogenesis.

Acknowledgment

This work is supported by the Natural Science Foundation of China (Grant Nos. 21273095, 20903045, 21203072).

Appendix A. Supplementary data

Supplementary data to this article can be found online at http://dx.doi.org/10.1016/j.bpc.2014.02.002.

References

[1] F. Chiti, C.M. Dobson, Protein misfolding, functional amyloid, and human disease, Annu. Rev. Biochem. 75 (2006) 333–366.
[2] C.M. Dobson, Protein folding and misfolding, Nature 426 (2003) 884–890.
[3] W.S. Gosal, I.J. Morten, E.W. Hewitt, D.A. Smith, N.H. Thomson, S.E. Radford, Competing pathways determine fibril morphology in the self-assembly of β_2-microglobulin into amyloid, J. Mol. Biol. 351 (2005) 850–864.
[4] J.I. Guijarro, M. Sunde, J.A. Jones, I.D. Campbell, C.M. Dobson, Amyloid fibril formation by an SH3 domain, Proc. Natl. Acad. Sci. 95 (1998) 4224.
[5] F. Chiti, N. Taddei, M. Bucciantini, P. White, G. Ramponi, C.M. Dobson, Mutational analysis of the propensity for amyloid formation by a globular protein, EMBO J. 19 (2000) 1441–1449.
[6] A.D. Ferrão-Gonzales, S.O. Souto, J.L. Silva, D. Foguel, The preaggregated state of an amyloidogenic protein: hydrostatic pressure converts native transthyretin into the amyloidogenic state, Proc. Natl. Acad. Sci. 97 (2000) 6445.
[7] D.J. Selkoe, Folding proteins in fatal ways, Nature 426 (2003) 900–904.
[8] H.L. Monaco, M. Rizzi, A. Coda, Structure of a complex of two plasma proteins: transthyretin and retinol-binding protein, Science 268 (1995) 1039–1041.
[9] A. Wojtczak, J. Luft, V. Cody, Mechanism of molecular recognition. Structural aspects of 3, 3'-diiodo-L-thyronine binding to human serum transthyretin, J. Biol. Chem. 267 (1992) 353–357.
[10] D.R. Jacobson, R.D. Pastore, R. Yaghoubian, I. Kane, G. Gallo, F.S. Buck, J.N. Buxbaum, Variant-sequence transthyretin (isoleucine 122) in late-onset cardiac amyloidosis in black Americans, N. Engl. J. Med. 336 (1997) 466–473.
[11] P. Westermark, K. Sletten, B. Johansson, G.G. Cornwell, Fibril in senile systemic amyloidosis is derived from normal transthyretin, Proc. Natl. Acad. Sci. 87 (1990) 2843.
[12] S. Mitsuhashi, M. Yazaki, T. Tokuda, Y. Sekijima, Y. Washimi, Y. Shimizu, Y. Ando, M.D. Benson, S.I. Ikeda, Biochemical characteristics of variant transthyretins causing hereditary leptomeningeal amyloidosis, Amyloid 12 (2005) 216–225.
[13] T.R. Foss, R.L. Wiseman, J.W. Kelly, The pathway by which the tetrameric protein transthyretin dissociates, Biochemistry 44 (2005) 15525–15533.
[14] A. Quintas, D.C. Vaz, I. Cardoso, M.J.M. Saraiva, R.M.M. Brito, Tetramer dissociation and monomer partial unfolding precedes protofibril formation in amyloidogenic transthyretin variants, J. Biol. Chem. 276 (2001) 27207.
[15] V.L. Shnyrov, E. Villar, G.G. Zhadan, J.M. Sanchez-Ruiz, A. Quintas, M.J.M. Saraiva, R.M. Brito, Comparative calorimetric study of non-amyloidogenic and amyloidogenic variants of the homotetrameric protein transthyretin, Biophys. Chem. 88 (2000) 61–67.
[16] Y. Liang, S.Z. Jasbi, S. Haftchenary, S. Morin, D.J. Wilson, Binding interactions in early-and late-stage amyloid aggregates of TTR < sub > (105–115)</sub>, Biophys. Chem. 144 (2009) 1–8.
[17] J.R. Rodrigues, C.J.V. Simões, C.G. Silva, R.M.M. Brito, Potentially amyloidogenic conformational intermediates populate the unfolding landscape of transthyretin: insights from molecular dynamics simulations, Protein Sci. 19 (2010) 202–219.
[18] M. Yang, B. Yordanov, Y. Levy, R. Brüschweiler, S. Huo, The sequence-dependent unfolding pathway plays a critical role in the amyloidogenicity of transthyretin, Biochemistry 45 (2006) 11992–12002.
[19] Q. Xue, J.-L. Zhang, Q.-C. Zheng, Y.-L. Cui, L. Chen, W.-T. Chu, H.-X. Zhang, Exploring the molecular basis of dsRNA recognition by Mss116p using molecular dynamics simulations and free-energy calculations, Langmuir 29 (2013) 11135–11144.
[20] Y.-L. Cui, Q.-C. Zheng, J.-L. Zhang, Q. Xue, Y. Wang, H.-X. Zhang, Molecular dynamic investigations of the mutational effects on structural characteristics and tunnel geometry in CYP17A1, J. Chem. Inf. Model. 53 (2013) 3308–3317.
[21] Y.L. Cui, J.L. Zhang, Q.C. Zheng, R.J. Niu, Y. Xu, H.X. Zhang, C.C. Sun, Structural and dynamic basis of human cytochrome P450 7B1: a survey of substrate selectivity and major active site access channels, Chem. Eur. J. 19 (2013) 549–557.
[22] S. Chakraborty, B. Chatterjee, S. Basu, A mechanistic insight into the amyloidogenic structure of hIAPP peptide revealed from sequence analysis and molecular dynamics simulation, Biophys. Chem. 168 (2012) 1–9.
[23] Z. Lai, W. Colón, J.W. Kelly, The acid-mediated denaturation pathway of transthyretin yields a conformational intermediate that can self-assemble into amyloid, Biochemistry 35 (1996) 6470–6482.
[24] D.R. Jacobson, D.E. McFarlin, I. Kane, J.N. Buxbaum, Transthyretin Pro 55, a variant associated with early-onset, aggressive, diffuse amyloidosis with cardiac and neurologic involvement, Hum. Genet. 89 (1992) 353–356.
[25] D. Studio, version 2.5, Accelrys, 2009. (in).
[26] W.T. Chu, Y.J. Wu, J.L. Zhang, Q.C. Zheng, L. Chen, Q. Xue, H.X. Zhang, Constant pH Molecular Dynamics (CpHMD) and mutation studies: insights into AaegOBP1 pH-induced ligand releasing mechanism, Biochim. Biophys. Acta Protein. Proteomics 1824 (2012) 913–918.
[27] S.L. Williams, C.A.F. De Oliveira, J.A. McCammon, Coupling constant pH molecular dynamics with accelerated molecular dynamics, J. Chem. Theory Comput. 6 (2010) 560–568.
[28] J. Mongan, D.A. Case, J.A. McCammon, Constant pH molecular dynamics in generalized Born implicit solvent, J. Comput. Chem. 25 (2004) 2038–2048.
[29] D. Case, T. Darden, T. Cheatham III, C. Simmerling, J. Wang, R. Duke, R. Luo, R. Walker, W. Zhang, K. Merz, AMBER 11, 142University of California, San Francisco, 2010.
[30] Y. Duan, C. Wu, S. Chowdhury, M.C. Lee, G. Xiong, W. Zhang, R. Yang, P. Cieplak, R. Luo, T. Lee, A point-charge force field for molecular mechanics simulations of proteins based on condensed-phase quantum mechanical calculations, J. Comput. Chem. 24 (2003) 1999–2012.
[31] V. Tsui, D.A. Case, Theory and applications of the generalized Born solvation model in macromolecular simulations, Biopolymers 56 (2000) 275–291.
[32] A. Onufriev, D. Bashford, A. David, Modification of the generalized Born model suitable for macromolecules, J. Phys. Chem. B 104 (2000) 3712–3720.
[33] A. Onufriev, D.A. Case, D. Bashford, Effective Born radii in the generalized Born approximation: the importance of being perfect, J. Comput. Chem. 23 (2002) 1297–1304.
[34] J. Shao, S.W. Tanner, N. Thompson, T.E. Cheatham III, Clustering molecular dynamics trajectories: 1. Characterizing the performance of different clustering algorithms, J. Chem. Theory Comput. 3 (2007) 2312–2334.
[35] W.L. DeLano, The PyMOL Molecular Graphics System, DeLano Scientific LLC, San Carlos, CA, USA, 2002.
[36] E.F. Pettersen, T.D. Goddard, C.C. Huang, G.S. Couch, D.M. Greenblatt, E.C. Meng, T.E. Ferrin, UCSF Chimera—a visualization system for exploratory research and analysis, J. Comput. Chem. 25 (2004) 1605–1612.
[37] A. Amadei, M.A. Ceruso, A. Di Nola, On the convergence of the conformational coordinates basis set obtained by the essential dynamics analysis of proteins' molecular dynamics simulations, Proteins Struct. Funct. Bioinforma. 36 (1999) 419–424.
[38] A. Amadei, A. Linssen, H.J. Berendsen, Essential dynamics of proteins, Proteins Struct. Funct. Bioinforma. 17 (1993) 412–425.
[39] A. Bakan, L.M. Meireles, I. Bahar, ProDy: protein dynamics inferred from theory and experiments, Bioinformatics 27 (2011) 1575–1577.
[40] W. Humphrey, A. Dalke, K. Schulten, VMD: visual molecular dynamics, J. Mol. Graph. 14 (1996) 33–38.
[41] J. Sørensen, D. Hamelberg, B. Schiøtt, J.A. McCammon, Comparative MD analysis of the stability of transthyretin providing insight into the fibrillation mechanism, Biopolymers 86 (2007) 73–82.
[42] A.A. Serag, C. Altenbach, M. Gingery, W.L. Hubbell, T.O. Yeates, Arrangement of subunits and ordering of β-strands in an amyloid sheet, Nat. Struct. Mol. Biol. 9 (2002) 734–739.